Jam Propagation Analysis With Mesoscopic Traffic Simulation

Balázs Varga and Tamás Tettamanti

Abstract— Road traffic simulation is becoming more important as the complexity and multi-modality of traffic grow with the evolution of novel transportation and automotive technologies. There are several ways to mimic traffic dynamics. However, realistic modeling traffic has a clear trade-off between accuracy and simulation processing time. Obviously, the more detailed traffic dynamics are sought, the more calculation is needed. The paper offers a compromise solution introducing a novel mesoscopic traffic simulation framework applicable on an arbitrary network level. The mathematical background of the simulation is provided as the extension of the shockwave profile model (SPM), distinguishing three continuous traffic states on a link. Extension of the model is done by means of a weighted directed graph where the dynamic edge weights are the queue lengths on each link. The model can handle both signalized and unsignalized road links. An important opportunity of the proposed network SPM approach is the analysis of traffic jam propagation and bottleneck detection. The presented mesoscopic simulator is validated based on both synthetic and real-world traffic networks using fleet traffic data. The simulated queue length in the mesoscopic simulation accurately matches the microscopic traffic simulation results.

Index Terms— Traffic modeling, Shockwave profile model, Jam propagation analysis.

I. INTRODUCTION

INITIALLY, traffic simulation was used by civil engineers to support infrastructure development through modeling traffic assignment [1], evaluating and optimizing road capacity [2], [3], optimizing intersection layouts, and signal programs [4], [5]. With the increase of various ITS solutions, traffic modeling and simulation also have emerged in different traffic estimation and control solutions [6], [7], [8], [9] as well as driver assistance systems [10], [11]. Moreover, the model-based approach allows for the assessment of theoretical scenarios and long-term forecasting. Obviously, the future of traffic simulation is the real-time simulation of large-scale traffic networks tending towards the digital-twin

technology [12], [13], [14], [15]. The more, a new notion, called "co-simulation", was recently born by the advent of the technology developments for Connected and Autonomous Vehicles, in which traffic simulation has also appeared beside the detailed vehicle dynamics modeling. [16], [17], [18], [19], [20], [21] introduced integrated testing frameworks for traffic and vehicle co-simulation for Connected and Autonomous Vehicles (CAVs). In these applications, the simulation performance is of crucial importance: as real-world or faster than real-world testing is expected for future homologation processes of CAVs [22], [23], [24]. Therefore, traffic simulation with high real-time factor is increasingly important. Accordingly, a mesoscopic traffic modeling approach that is capable of capturing traffic patterns is introduced for efficient, at the same time, realistic traffic simulation. In the paper, the efficiency of the mesoscopic model will be shown for jam propagation analysis. Before delving into jam propagation, traffic modeling as a preliminary tool is outlined.

A. Traffic Modeling

Generally, road traffic simulation is categorized according to the level of detail of the applied traffic modeling, i.e., microscopic, mesoscopic, and macroscopic levels of simulation [25]. Each category has a trade-off between accuracy and computational demand and has its specific use cases.

Microscopic models describe the traffic flow in a detailed manner, using the dynamics of individual vehicles. Car following models are the most common type of microscopic traffic models. They describe the driver's behavior concerning the preceding vehicle in the same lane. Safe distance models describe the dynamics of a single vehicle in relation to its predecessor [26], [27], [28], [29]. Stimulus-response models represent the vehicle's dynamics based on the observed behavior of the preceding vehicle [30]. Cellular automaton models (such as the cell transmission model (CTM) [31]) divide the space into equally sized cells. It then describes the movement of vehicles from cell to cell in a discrete way [32]. This fine-grained approach also extends to the road infrastructure (e.g., lane description, traffic lights), thus able to model complex traffic phenomena such as traffic jam propagation. On the other hand, the accuracy of the model is a mixed blessing. The complexity of car following models makes calibration tedious and have significant impact on road capacity [33]. Thus, achieving realistic jam propagation results with microsimulation requires large effort. Additionally,

large-scale models are resource intensive to simulate, limiting real-time capabilities.

Mesoscopic traffic models are an intermediate description of road traffic, where the movements of individual vehicles are neglected, and clusters of vehicles are considered. A cluster of vehicles is a homogeneous group of vehicles that share a specific property such as size and average velocity [25]. The behavior of individual vehicles is described as stochastic variables [34]. Gas-kinetic models employ equations from fluid dynamics to describe traffic flow as a homogeneous continuum [35], [36]. Thus, mesoscopic models are capable of capturing the fluctuation of traffic (i.e., jam formation and dissipation) in an aggregated way, thus being easier to calibrate (sensitive to only a few parameters) and computationally more efficient.

Macroscopic models ignore individual parameters of vehicles, and the flow of traffic is described with hourly aggregates such as traffic mean speed, traffic density, and traffic volume on road link (or sub-network) level. The first macroscopic flow model is proposed by [37]. The fundamental equation of traffic flow is shaped by choice of the velocity equation, e.g., [38] and [39]. Besides the above macro models (mainly applicable on freeways or arterial roads), it is important to distinguish another group of macroscopic models, also called transportation forecasting or four-step travel model [40]. Although dynamic macroscopic models exist as well, they are rather used to model the rerouting behavior of traffic. The main limitation of the macroscopic modeling approach is the absence of vehicle dynamics.

B. Jam Propagation Analysis

Traffic jam propagation or percolation analysis studies how congestion on a roadway spreads and affects other sections of the road network. There have been several approaches to studying this phenomenon distinguishing highway and urban traffic jam propagation. In road traffic, bottlenecks are defined as locations where traffic demand exceeds capacity. The question of jam propagation is the effect of such bottlenecks in terms of queue lengths, spillback (gridlock), and travel time delays.

Due to the complex nature of the topic, instead of analytical methods (or simple models), highly complex, modular models, i.e., simulators are preferred. The more, such model-based simulators are more desirable as opposed to data-driven approaches since traffic jams are often caused by one-off events (e.g., accidents, roadworks, public events, etc.) and cannot be reliably evaluated from the data. Additionally, hypothetical scenarios (such as changing a traffic light program) can only be tested through models.

Several authors have explored different aspects of traffic jam propagation analysis through traffic modeling, simulation, and empirical data. References [41] and [42] take a macroscopic approach to analyze gridlock formation and dissipation dynamics. The authors of [43], [44], and [45] analyze jam propagation through network theory. They evaluate the severity of the jam by clustering them. However, the results can only isolate bottlenecks and do not give insight into the dynamics of jam propagation. Only a few studies deal with the

cause-and-effect analysis of traffic bottlenecks. Reference [46] defined a tree structure to represent jam propagation in a probabilistic way. Reference [47] create a directed graph of the road network to find congestion propagation paths using traffic measurements. Reference [48] uses the topology of the network to assess queue growth. Reference [49] construct propagation graphs to identify the causal relationship between congestion at different road segments by calculating congestion costs. References [46] and [50] discretize the network into regions, not on a link level. Thus, they cannot analyze spillbacks and recursive effects. Many works use big data analysis to find traffic patterns, e.g., [51] and [52]. However, it is hard to find the causes of jams without a model. Reference [53] uses the CTM to estimate vehicle speed and identify bottlenecks. Thus, congestion is categorized by average velocity instead of queues. On the other hand, in urban areas, traffic flow is mainly actuated by traffic lights inducing queues and shockwaves. Thus, we hypothesize that a traffic model focusing on queue growth and dissipation can deliver more accurate results for jam propagation modeling than other aggregate models, such as the CTM.

C. Contribution

This paper proposes a mesoscopic traffic model to find bottlenecks and analyze queue growth. The shockwave profile model (SPM, [54]) is extended to a network level, capable of handling multiple signalized and unsignalized road links. Until now, the SPM has not been extended to urban networks. Thus the first contribution of the paper is a fully functional mesoscopic traffic simulator capable of handling both signalized and unsignalized intersections.

The SPM separates each link into three continuous regions: free flow, moving queue, and stationary queue. Jam propagation is assessed by means of these traffic regions. Thus, as a second contribution, we give a purpose to the proposed simulator without excessively customizing it for that objective. Compared to other works in percolation analysis, we use a model-based approach, not a data-driven one. This makes cause and effect analysis simpler too. The proposed mesoscopic model is more resource-efficient compared to microscopic traffic simulation but captures traffic dynamics better than macroscopic models. The model defines the road network as a directed graph and needs only a few inputs (inflows, turning rates), making it an efficient tool for web-based applications too. Additionally, the mesoscopic model can be calibrated solely relying on abundantly available floating car data.

The paper is structured as follows. Section II outlines the shockwave profile model and extends it to an urban traffic network. Then, Section II-C provides a methodology to analyze jam propagation and traffic bottlenecks using the network SPM. Section III discusses the calibration and usage of the model through a synthetic grid network where it is benchmarked against other contemporary models. Additionally, its capabilities are tested to capture the spillback phenomenon on a real road section, calibrated with floating car data. Finally, IV concludes the results of the paper and provides further outlook on the usage of the model.
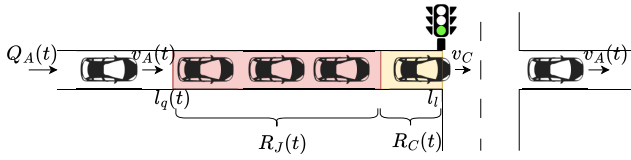
Fig. 1. Traffic flow states in front of a signalized intersection.

Fig. 2. Shockwave profiles at a signalized intersection.

II. NETWORK SHOCKWAVE PROFILE MODEL

This section presents the shockwave profile model at signalized link level. Then, it is extended to the network level, resulting in a mesoscopic traffic simulator. The section also discusses the case of unsignalized intersections in the proposed modeling framework.

Fig. 3. Three different MFDs with the queuing shockwave W_1, the queue discharge shockwave W_2, and the departure shockwave W_3 velocities.

A. Shockwaves at a Signalized Intersection

The shockwave profile model was first introduced in [55] and further studied in [54] for signalized road links. The SPM model exclusively works with traffic flow volumes and queue lengths, i.e., treating vehicles as a continuum instead of individual agents. It describes traffic states in such links, distinguishing three states:

- Free flow farther upstream the traffic light, where the average velocity is v_A. Additionally, the traffic density is assumed to be ρ_A. Thus, the traffic flow is $Q_A = \rho_A v_A$.
- Stationary queue (R_J) in front of the traffic light, $v_J = 0$. Since the traffic is stationary, there is no traffic flow ($Q_J = 0$) and the traffic is at jam density, ρ_J.
- Moving queue (R_C): drivers cross the traffic light at green with the critical velocity v_C, (as a rule of thumb: 0.5 vehicles per second, i.e., $Q_C = 1800 \frac{veh}{h}$ per lane). Additionally, the traffic density at this state is denoted with ρ_C.

Figure 1) depicts these regions with l_l being the link length and l_q being the queue length. The traffic inflow is denoted with Q_A.

In the SPM, boundaries of the traffic regions (R_A, R_C) upstream a signalized intersection are governed by shockwaves. The model distinguishes four shockwaves:

- **Queuing shockwave velocity,** $W_1(t)$ is formed by vehicles accumulating at the red light. Vehicles stopping at the tail of the queue from their actual velocity to zero forms a shockwave.

$$W_1(t) = -\frac{Q_A(t)}{\rho_J - \rho_A(t)}. \tag{1}$$

- **Discharge shockwave velocity,** W_2 is time-independent. In the fundamental diagram, the discharge shockwave velocity is the slope of the line connecting the jam density and the critical density.

$$W_2 = \frac{Q_C}{\rho_J - \rho_C}. \tag{2}$$

- **Departure wave velocity** $W_3(t)$ is generated as the queue dissipates as vehicles leave the intersection at green. It starts at the intersection of the queuing and discharge
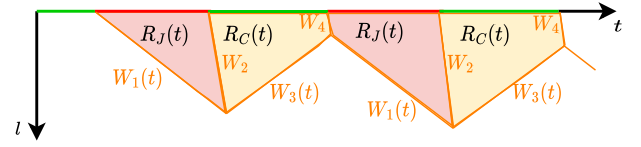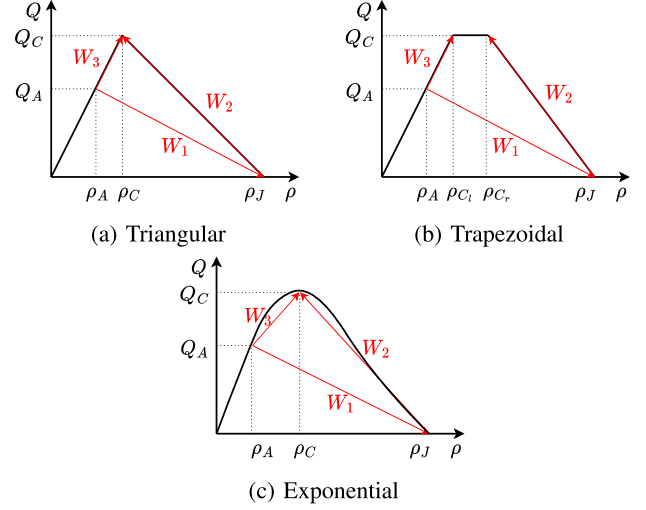
shockwaves. In addition, newly arrived vehicles feed the queue and hence

$$W_3(t) = \frac{Q_C - Q_A(t)}{|\rho_C - \rho_A(t)|}. \tag{3}$$

Assuming a triangular link fundamental diagram, the departure wave velocity becomes constant. Additionally, in the case when the inflow is larger than the peak capacity ($Q_A > Q_C$), the shockwave changes sign, leading to a growing queue, i.e., the queue is fed faster than it can dissipate.

- **Pressure wave velocity** W_4 separates a critical density and a jam density region, and it has the same speed as the discharge wave. The pressure wave is only present if there is a residual queue, i.e., the queue cannot fully discharge during a green interval

$$W_4 = -\frac{Q_C}{\rho_J - \rho_C}. \tag{4}$$

Shockwave velocities can be represented in time-space diagram (Figure 2) and on the Macroscopic Fundamental Diagram (MFD) too (Figure 3).

The shockwave profile model defines traffic state transitions based on specific points of the macroscopic fundamental diagram (MFD). However, the MFD can take different shapes, significantly affecting the slope of each shockwave. Consider Figure 3 for three different examples. The triangular MFD is the simplest one, where the average velocity is constant in the uncongested case. The trapezoidal MFD offers an additional degree of freedom in calibration by assigning the peak capacity Q_C to several density levels. In the SPM, this allows selecting the discharge wave velocity more freely, resulting in more

accurate mesoscopic modeling. Finally, the exponential MFD forms a nonlinear relationship between traffic density and flow. In this case, the departure shockwave velocity is sensitive to the traffic inflow Q_A.

Using the model, it is possible to compute the queue length on a link continuously. Assuming $l_{W_1}(t)$, $l_{W_2}(t)$, $l_{W_3}(t)$, $l_{W_4}(t)$ are the shockwave lengths for each shockwave, their evolution can be given as:

$$l_{W_1}(t + \Delta t)$$
$$= \begin{cases} l_{W_4}(t) + W_1(t)\Delta t & if \ l_{W_3}(t) < l_{W_4}(t), \\ min(l_{W_1}(t) + W_1(t)\Delta t, \ l_l) & if \ l_{W_1}(t) > l_{W_2}(t) \\ & or \ (red \ and \ l_{W_4} = 0), \\ 0 & otherwise, \end{cases} \tag{5}$$

$$xl_{W_2}(t + \Delta t)$$
$$= \begin{cases} l_{W_2}(t) + W_2(t)\Delta t & if \ green \ and \ l_{W_1}(t) > l_{W_2}(t), \\ 0 & otherwise, \end{cases} \tag{6}$$

$$l_{W_3}(t + \Delta t)$$
$$= \begin{cases} l_{W_2}(t) + W_3(t)\Delta t & if \ l_{W_1}(t) < l_{W_2}(t), \\ max(l_{W_3}(t) + W_3(t)\Delta t, \ 0) & if \ l_{W_3}(t) > l_{W_4}(t), \\ 0 & otherwise, \end{cases} \tag{7}$$

$$l_{W_4}(t + \Delta t)$$
$$= \begin{cases} l_{W_4}(t) + W_4(t)\Delta t & if \ red \ and \ l_{W_3}(t) > 0, \\ 0 & otherwise. \end{cases} \tag{8}$$

Finally, the queue length on the link is

$$l_q(t) = max(l_{W_1}(t), \ l_{W_3}(t)), \quad 0 \le l_q(t) \le l_l. \tag{9}$$

Note that the queue length is bounded between $[0, l_l]$ as it cannot be negative or exceed the length of the link. Consequently, if the length of the free flow region $(l_l - l_q(t))$, the stationary queue $(l_{W_1}(t) - l_{W_2}(t))$, and the moving queue $(l_q(t) - (l_{W_1}(t) - l_{W_2}(t)))$ can be obtained. From that, macroscopic traffic variables such as (space) mean speed and density can be obtained for the full link by weighted averaging the fixed macroscopic variables (v_A, v_J, and v_C, and ρ_A, ρ_J, ρ_C, respectively).

Additionally, if the traffic program and the vehicle inflow are constant or known for future steps, it is possible to perform short-term prediction of traffic states and queue lengths [34].

The model considers the time needed by vehicles to reach the tail of the queue. Based on the free length of the link $(l_f = l_l - l_q)$ and the average velocity of free flow vehicles v_A, the flows feeding the queue are delayed by $t_{del} = \frac{l_f}{v_A}$. This approach to handling the delay is similar to how it is dealt with in the delayed CTM [31].

Remark 1: The model can be extended to handle stochastic (but ergodic) vehicle arrival patterns, resulting in probabilistic queue lengths (and probabilistic jam propagation in the network model sense), see [34].

Remark 2: Queue lengths can be given in passenger car equivalents (PCE) too:

$$n_q(t) = l_q(t)/l_{pce}, \tag{10}$$

with l_{pce} being the average length of a car. Then, the number of vehicles entering $n_{in}(c)$ and exiting $n_{out}(c)$ a link during one traffic light cycle (denoted by c) is

$$n_{in}(c) = \int_t^{t+t_{cyc}} \frac{Q_1(\tau)}{3600} d\tau, \tag{11}$$

and

$$n_{out}(c) = min\left(n_q(t), \int_0^{t_{green}} \frac{W_2}{l_{pce}} d\tau\right), \tag{12}$$

with t_{green} being the green time within cycle time t_{cyc}. Then, the evolution of queue length in one traffic light cycle is

$$n(c + 1) = n(c) + n_{in}(c) - n_{out}(c). \tag{13}$$

This discrete-time model is similar to the store-and-forward model with link-level spatial and cycle-time level temporal discretization [56]. Similarly, Eqs. (11)-(13) can be used for sub-cycle time intervals ($\Delta t < c$) too.
Based on the above, the outflow can be given as follows:

$$Q_{out}(t) = \begin{cases} 0 & if \ red \ or \\ & downstream \ jammed, \\ Q_C & if \ l_{W_2}(t) > 0, \\ Q_A(t - t_{del}) & if \ l_q = 0. \end{cases} \tag{14}$$

If two similar links are connected, the vehicle inflow to the second link will be the Q_C of the first one during a green phase. That means the velocities W_1 and W_2 will be similar, and W_3 becomes zero. Therefore, inflow and outflow are similar if both traffic lights are green; thus, the queue length is constant. Additionally, if the downstream link is jammed, the outflow is prevented from the link. This assumption is further evaluated in the sequel when extending the model to the network level.

B. Network SPM

The link SPM model in the previous section can be turned into a network by interconnecting individual links. The network SPM model is based on a directed graph. Road links are the edges, and intersections are assumed to be nodes. At each intersection (node), outflow from adjacent links can be used as inflow to the current ones. Vehicle flows are distributed based on turning ratios. Then, the queue lengths are computed based on the SPM for each link. With this approach, a whole traffic network with traffic lights can be modeled. The SPM model can estimate queue lengths which can be used to detect spillover, gridlock, and disturbance propagation. There is spillover if this queue length is greater or equal to the length of the link ($l_l \le l_q$). If that happens, the source node of this link gets blocked, preventing outflow from every edge that ends in that node. That is to model gridlocked intersections.

Using the layout in Figure 4, The traffic inflow to Link X is the weighted sum of the outflows from the upstream links:

$$Q_X(t) = Q_Y(t)\alpha_Y + Q_Z(t)\alpha_Z + Q_W(t)\alpha_W, \tag{15}$$

with $\alpha_{X,Y,Z,W}$ being the turning rates, and $Q_{X,Y,Z,W}$ are the traffic flows, respectively. Thus, the model assumes the information on turning rates at each intersection. This is a

Fig. 4. Shockwave profile model on network level.

Fig. 5. Flowchart of traffic jam assessment.

common, practical assumption for network-level traffic models (e.g., [56], [57]), and can be obtained from OD matrices via traffic assignment algorithms, e.g., [58]. Additionally, the perimeter inflows of the network and the signal program are needed.

Since most road networks consist of not only signalized intersections, unsignalized links are considered too. In the absence of traffic lights, shockwaves are not triggered. In this case, a different approach has to be taken: gap acceptance [59].

Based on the works of [60] and [61], links with lower priority (minor flow, Q^-) can be modeled as a continuous queueing process depending on the flow of the higher priority road (major flow, Q^+).

$$Q^- = \frac{1}{t_f} e^{-t_c Q^+}, \tag{16}$$

where t_f is the follow-up time, and t_c is the critical gap. The value of t_c and t_f depend on the type of the intersection (e.g., turning left or right), [62]. The shockwave profile model can also be interpreted in this case to a lesser extent. Since vehicles are leaving the minor road with a given rate (not necessarily Q_C), and there are vehicles feeding the moving queue, a permanent dissipation wave (W_3) is present. Trivially, the queue length on links ending with right-of-way signs is also saturated: it cannot be negative or longer than the link length.

Remark 3: Roundabouts can be modeled with this approach too. Sections of the roundabout are road links with priority, while the legs of the roundabout are minor roads. This is assuming drivers inside the roundabout have the right-of-way.

C. Bottleneck Assessment Methodology

The SPM is designed to model queues on a road link. The queue length on a link alone is a piece of valuable information in detecting congested roads. The network model is capable of the more ambitious task of assessing jam propagation dynamics too. The network model is built as a directed graph, with each edge being a road link where queue length evolution is continuously evaluated. If one link gets full, it affects the upstream links too via blocking traffic flow in the upstream intersection (node) completely. Thus, the order in which links get congested can quickly be evaluated. Critical links and the causality of jams can be traced back. The main difference compared to [47] is that congestion paths are obtained through

Fig. 6. Graph representation of the grid case study network.

a traffic model rather than sparse measurements. The model allows us to find bottlenecks by means of arbitrary traffic blockages and fictitious traffic flows. Additionally, short-term traffic state predictions can be made using the mesoscopic model to forecast gridlocks and take preventive action.

As stated in Section II-B, if an edge gets congested, it entirely blocks the outflow traffic of all of its upstream neighbors. When constructing the network graph, one might need to split an intersection into smaller ones, e.g., define a node at each turning (merging, splitting) point. That is to better asses which directions get congested.

Some particular use-cases of the model that will be elaborated in the case studies are

- **Incident detection.** If traffic conditions abruptly change due to an external event (e.g., accident, construction), queue forming and dissipating patterns will change. In most practical cases, this means a capacity drop, resulting in unexpected traffic jams, which can be modeled with the SPM.
- **Hotspot detection.** When jams occur recurrently, they can stem from various reasons, e.g., incorrect traffic light programs, insufficient capacity of turning lanes, or other types of traffic bottlenecks. Via modeling the propagation of queues, these bottlenecks can be traced back.

The above traffic network inefficiencies are systematically analyzed through the following metrics: the number of links affected and the order in which they get congested (congestion path or congestion propagation graph [49]). The cumulated length of the jam is the sum of queue lengths in the congestion path. The cumulated length is related to the severity of the

Fig. 7. Hourly traffic flow on the evaluated links in the grid network for every scenario and every benchmark.

congestion. Additionally, the queue growth rate (the cumulated length derivative) is also analyzed.

III. CALIBRATION, VALIDATION, AND USE CASES

In the sequel, two traffic networks are constructed based on the SPM. First, a 3-by-3 grid network is implemented with traffic lights, right-of-way intersections, and an accident to check jam propagation in the network. The grid network is used to validate and benchmark the mesoscopic model against SUMO microsimulation (using the default settings), the mesosimulation option of SUMO [63], and against the delayed- and non-delayed versions of the cell transmission model [31]. Then, a real-world arterial road is modeled and calibrated using TomTom fleet data. This case study is particularly interesting because, during peak hours, there is a left-turning lane that usually gets congested, blocking the forward-going traffic too. Additionally, an accident is modeled in this network as an alternate source of jam. The methodology of jam propagation analysis via the SPM is shown in Figure 5.

A. Grid Network

A 3-by-3 grid road network with one-way streets is modeled for validation, see Figure 6. Each intersection is modeled as a node in the graph-based representation of the network. Note that a more detailed description is possible in more complex intersections (e.g., a distinct edge for each lane). This network has two variants: one with traffic lights and one with right-of-way streets where vertical roads have priority over the horizontal ones. Based on [64], the gap acceptance parameters for minor flow roads are $t_f = 2.8$ and $t_c = 4.1$. In the traffic light variant, the traffic cycle is 60 s long with 30 s green intervals. Signal controllers are calibrated such that the vertical directions have a green wave. Each link is 250 m long, and the speed limit is 50 km/h. In the model, trapezoidal MFDs are used with the jam density being $\rho_J = 150 \ veh/km/lane$, the peak capacity is $Q_C = 1800 \ veh/h/lane$ (stemming from the rule of thumb that a half vehicle can cross a signalized intersection each second, [62], [65], [66], [67]). The free flow velocity $v_f = 50 \ km/h$ and the offset between ρ_{C_l} and ρ_{C_r} is 40 veh/km. We used the same MFD for both the SPM and the benchmark CTMs. Each link was discretized into 50 m cells for the CTM. Simulations have been carried out with

link-sized cells, i.e., the link transmission model [68] too. However, no significant differences were observed between the two. Thus, in the sequel, only the results of the CTM are reported. The traffic inflow is 540 veh/h at every source node (A, C, M, T, R, H), and the turning rates are $50-50\%$ at each intersection.

For validation purposes, it is checked how many vehicles travel each link in both cases (Figure 7). Results suggest that the SPM underestimates traffic flow on the right-of-way links, while the CTM overestimates traffic flow in general. The mesoscopic model of SUMO cannot consider traffic lights or gridlock [69], thus completely failing in jam propagation analysis. The reason for underestimation in the SPM case stems from its queue-length focus rather than vehicle number focus, i.e., vehicle number is evaluated from queues, see Remark 2. On the other hand, the CTM overestimates traffic flow since it always assumes the road is utilized at its peak capacity and does not distinguish between moving and stationary queues.

In the unsignalized network, the roads with priority has zero queue length, which is well captured by every model. On the other hand, instantaneous queue lengths cannot be captured accurately by any of the models. Average queue lengths, however, can be captured by the SPM better than the CTM benchmarks, see Table II.

Next, the average queue lengths are analyzed for six links in the scenario with traffic lights (Figure 8). Both the CTM and SPM-based simulations capture the queue length fluctuation well in the links close to the entry of the network. On the other hand, accuracy degrades slightly for both the SPM and the CTM from left to right. Figures on the left (Link AG and HG) are close to the source nodes, while Links JQ and FE are three links downstream of the source. Thus, the inaccuracy stems from the accumulating modeling errors. This leads to the conclusion that modeling large-scale networks (without intermittent corrections) is only possible with limitations using the network SPM. Additionally, this accuracy degradation is more severe in the CTM cases. The mesoscopic SUMO simulation cannot produce realistic queues. Note that the shockwave profile model (and similar queuing models) often miss the maximum length of the queue [54].

Next, an accident is simulated in the signalized grid network blocking the exit of Node B. The question is how this accident propagates through the network, which links get congested
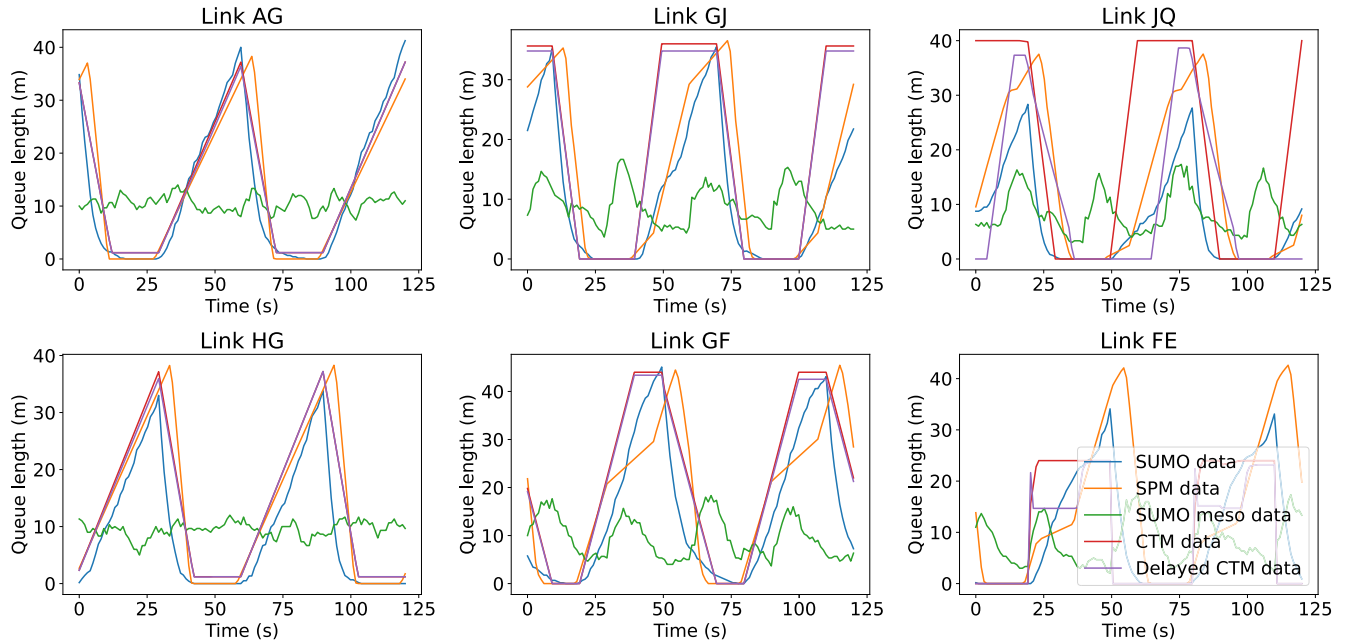
Fig. 8.   Queue length comparison at different links of the grid network with traffic lights. 120 seconds long slices (two traffic light cycles) of the whole simulation are averaged.

TABLE I

CONGESTION PATH IN THE GRID NETWORK. THE LINKS ARE ORDERED BY THE TIME INSTANT THEY GET BLOCKED (t_b)

SUMO		SPM		CTM		Delayed CTM	
Link	t_b (s)	Link	t_b (s)	Link	t_b (s)	Link	t_b (s)
FB	396	FB	276	FB	169	FB	244
KF	539	KF	482	GF	199	GF	310
GF	550	GF	501	KF	201	KF	337
AG	738	AG	713	PK	269	AG	358
PK	745	LK	717	AG	314	PK	389
HG	763	HG	735	LK	322	HG	417
LK	918	PK	736	QP	328	LK	434
TP	969	ML	944	HG	334	QP	447
ML	1153	TP	953	JQ	434	TP	496
QP	1203	EL	993	TP	441	JQ	508
EL	1301	QP	1092	EL	487	EL	612
RQ	1460	CE	1245	ML	581	ML	625
CE	1601	RQ	1353	RQ	614	RQ	662
		JQ	1669	GJ	675	GJ	776
				CE	741	CE	803

first, and how fast the jam grows. First, the direction of growth is analyzed. Table I summarizes in what order and at what time instant a link gets fully congested. The order in which the links get congested in the SPM is almost similar to the order modeled by SUMO. Noth that, however, there is a link (JQ) that gets blocked in the SPM and not in SUMO. Additionally, the SPM predicts faster queue growth. The CTM predicts much faster jam propagation and misses the order in which links get congested. Thus, neither the propagation speed nor the congestion propagation graph cannot be correctly reconstructed. The number of vehicles that could cross each link (Figure 7c) is in accordance with the result in Table I: the earlier a link gets blocked, the fewer vehicles could travel it. Finally, the cumulated queue length is shown in Figure 9. It can be seen that the network eventually gets to a steady state where the queue cannot grow any further.

The difference between the total queue length arises from Link JQ that gets congested in the SPM and not in SUMO. Additionally, the slope of the cumulated queue length is the rate of queue growth. The main difference in the queue growth speed can stem not only from modeling inaccuracy but from simplification too. If the queue length reaches the previous intersection, both the SPM and the CTM assumes that the node is entirely blocked, i.e., there is no flow from that node in any direction. However, depending on the topology of the intersection, it could be possible that there are still some directions vehicles can travel.

Finally, the RMSE for every link in every scenario is summarized in Table II. The RMSE results confirm the previous findings: queues are zero both in SUMO and in the SPM for the roads with priority. In the signalized case, links further downstream from the sources show higher errors. In the jam propagation scenario, Table II reports larger errors when the temporal difference in congestion time on a certain link (Table I) is larger.

B. Real Arterial Road

The second example is an arterial road in Budapest, towards the city center, that often gets congested in the morning peak due to commuting traffic. The situation gets especially severe at a left turning lane that gets congested, blocking the forward-going traffic too. The reason it gets congested is also edifying. Since the arterial is congested, navigation applications recommend detours towards a residential area to drivers, and the detour involves the said left turn too. Thus, the user optimum recommended by the application further degrades the system optimum.

The length of the left turning lane is 50 m, and the green time for this direction is 12 s in a 90 s traffic program cycle. There are two lanes that go forward towards the city center.

TABLE II

ROOT MEAN SQUARE ERROR OF QUEUE FOR THE SPM AND ITS BENCHMARKS COMPARED TO SUMO MICROSIMULATION IN THE GRID NETWORK

	Right of way				Traffic light				Jam propagation			
Link	SPM	CTM	del. CTM	SUMO meso	SPM	CTM	del. CTM	SUMO meso	SPM	CTM	del. CTM	SUMO meso
AG	0.026	0.027	0.027	0.23	0.242	0.225	0.227	0.351	0.224	1.217	1.064	2.041
GJ	0.0	0.02	0.02	0.215	0.227	0.31	0.309	0.302	0.082	3.079	2.983	0.264
JQ	0.0	0.02	0.02	0.206	0.24	0.201	0.203	0.23	3.114	0.08	0.081	0.22
QS	0.0	0.02	0.02	0.214	0.0	0.336	0.179	0.212	0.0	3.151	3.057	0.209
TP	0.025	0.027	0.027	0.22	0.203	0.666	0.297	0.296	0.162	1.589	1.467	2.095
PK	0.001	0.02	0.02	0.195	0.262	0.345	0.305	0.232	0.223	0.872	0.692	2.875
KF	0.0	0.02	0.02	0.187	0.21	0.486	0.48	0.233	0.408	1.181	1.021	2.907
FB	0.0	0.02	0.02	0.204	0.0	0.398	0.394	0.205	0.567	0.746	1.1	2.823
CE	0.025	0.027	0.027	0.221	0.275	0.354	0.352	0.36	1.155	1.879	1.791	2.149
EL	0.0	0.02	0.02	0.198	0.262	0.22	0.221	0.218	0.862	3.296	3.296	2.676
LO	0.0	0.02	0.02	0.212	0.196	0.481	0.332	0.247	0.113	3.138	3.042	0.243
OU	0.0	0.02	0.02	0.223	0.0	0.444	0.405	0.224	0.0	3.258	3.18	0.23
HG	0.776	0.711	0.711	0.65	0.199	0.24	0.241	0.281	0.162	0.962	0.695	2.05
GF	0.253	0.232	0.232	0.26	0.34	0.453	0.641	0.419	0.413	1.01	0.758	2.776
FE	0.331	0.309	0.309	0.312	0.253	0.326	0.286	0.309	0.089	0.433	0.422	0.577
ED	0.0	0.02	0.02	0.218	0.0	0.307	0.305	0.229	0.0	3.128	3.041	0.234
ML	0.112	0.186	0.186	0.227	0.221	0.268	0.28	0.285	0.745	3.388	3.396	2.06
LK	0.24	0.233	0.233	0.26	0.183	0.236	0.233	0.242	0.494	3.563	3.571	2.818
KJ	0.331	0.331	0.331	0.341	0.291	0.386	0.376	0.271	0.088	3.205	3.126	0.271
JI	0.0	0.02	0.02	0.209	0.0	0.066	0.065	0.208	0.0	0.066	0.065	0.199
RQ	0.343	0.313	0.313	0.325	0.217	0.743	0.721	0.265	0.501	1.799	1.653	2.631
QP	0.361	0.326	0.326	0.321	0.214	0.262	0.259	0.273	0.277	3.381	3.381	2.892
PO	0.401	0.419	0.419	0.404	0.252	0.288	0.286	0.317	0.105	3.11	3.029	0.258
ON	0.0	0.02	0.02	0.199	0.0	0.307	0.305	0.205	0.0	3.154	3.066	0.209
Avg.	0.139	0.141	0.141	0.261	0.179	0.348	0.321	0.267	0.408	2.112	2.041	1.488
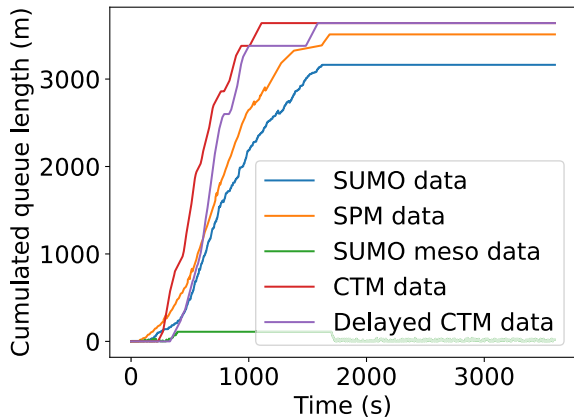
Fig. 9. Total queue length stemming from the blocked exit at Link FB in the grid network.
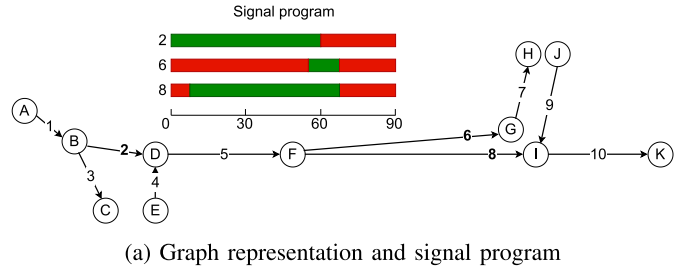
(a) Graph representation and signal program

(b) Aerial view of the road section (Source: Google Maps, GPS coordinates: 47.47448, 19.02532)

Fig. 10. Arterial road case study.

The legal speed limit is 50 km/h. The graph representation, the signal program, and the aerial view of the arterial road are shown in Figure 10. The said left turning lane is Link FG, and the forward going lane is Link FI in the graph. Note that Link BD is also signalized.

The model is calibrated using OD data from TomTom and traffic counts entering the said area. Based on the measurements, we consider two real and a fabricated scenario. In every scenario, the main inflow is 2400 veh/h. In the first scenario, 10% of the vehicles take the critical left turn, while in the second 15% (based on TomTom). In the third case, an accident is simulated 100 m downstream of the intersection. Table III summarizes origin-destinations for the scenarios.

Similar to previous experiments, the average queue lengths are first evaluated. See Figure 11. With 10% left turning

TABLE III

ORIGIN-DESTINATION FLOWS (VEH/H) IN THE ARTERIAL NETWORK WITH 10% LEFT-TURNING RATE (15% LEFT-TURNING RATE IN PARENTHESIS)

		To			
		C	H	K	$\sum$
From	A	480	192 (288)	1728 (1632)	2400
	E	0	0	70	70
	J	0	0	0	0
	$\sum$	480	192 (288)	1798 (1702)	

rate, the turning lane does not get congested, while the forward-going lanes do. That causes some spillback to Link DF. If the turning rate increases to 15%, the turning lane gets congested too. This causes more spillback to Link DF. Note
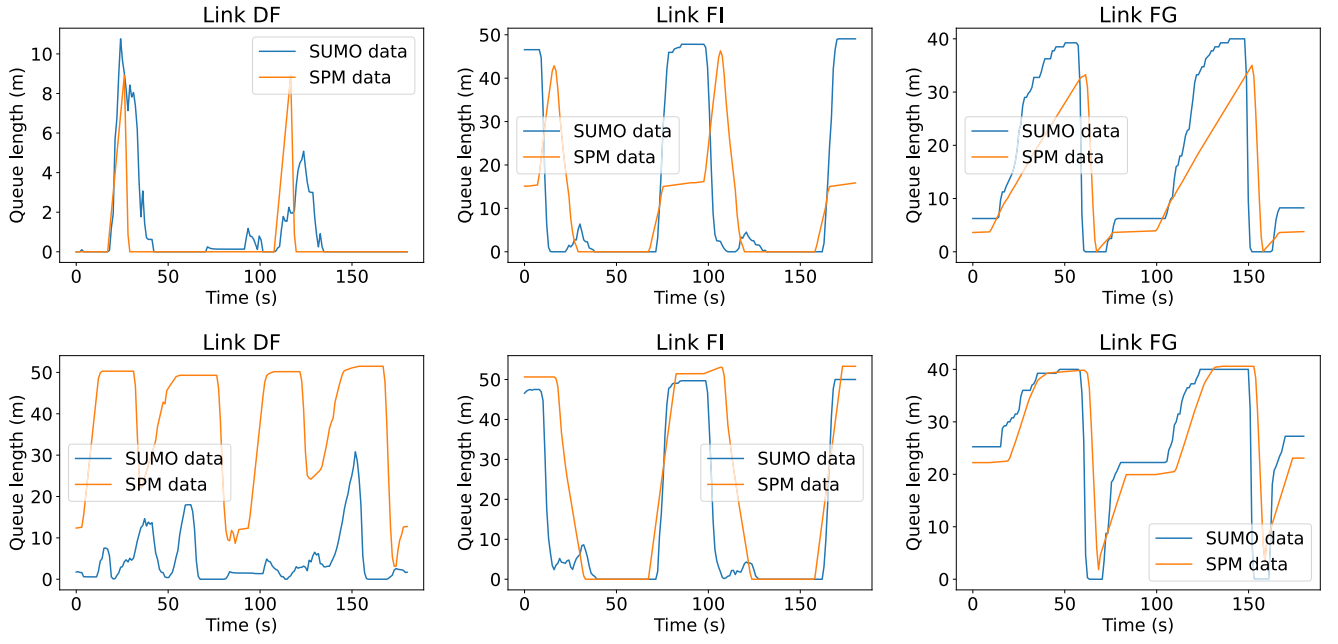
Fig. 11. Queue length comparison upstream the intersection with the critical left turn. Top figures depict the scenario with a turning rate of 10% left, the bottom figures depict a turning rate of 15%. Figures on the left show the road link prior the turning lane, figures in the middle show the queues on the link for vehicle going straight ahead, and figures on the right depict queuing on the left turning lane. 180 seconds long slices (two traffic light cycles) of the whole simulation are averaged.
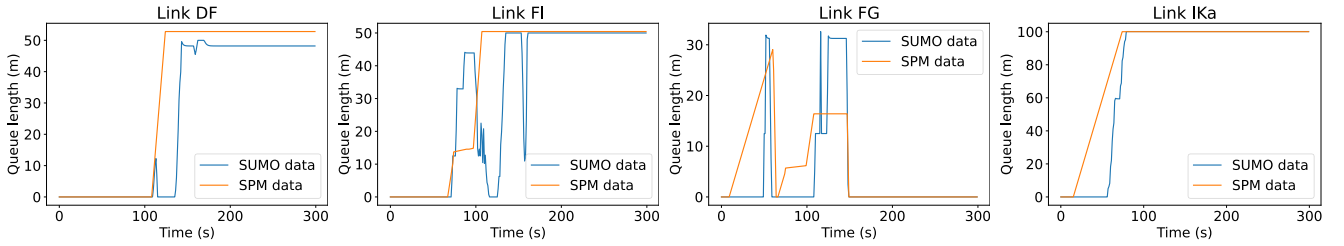
Fig. 12. Queue length comparison with an accident caused in the experimental network on each link.

TABLE IV
AVERAGE VELOCITIES (KM/H) UPSTREAM AND DOWNSTREAM THE CRITICAL INTERSECTION WITH DIFFERENT TURNING RATES

	TomTom	SUMO	SPM
Upstream (DF, FI), 10%	31.93	29.36	26.38
Downstream (IK), 10%	46.2	38.19	45.47
Upstream (DF, FI), 15%	37.25	33.20	39.15
Downstream (IK), 15%	43.42	40.88	47.61

that the spillback in the SPM is significantly larger than in SUMO. That is because if any of the links FI or FG gets congested, the outflow is blocked from DF. Since FI has two lanes, in SUMO, the vehicles that travel straight ahead can still use the rightmost lane even if vehicles are blocking the middle lane intending to change lanes to the left. Modeling such an unstable behavior is always challenging. Since gridlock happens at different times in the two simulators, its dissipation will show different patterns. Thus, even a small discrepancy can result in large differences. Alternatively, one could model the two-lane sections as two separate edges, modeling queues on them separately.

Next, as a validation step, average velocities reported by TomTom are compared to the average velocities in the mesoscopic and the microscopic simulation, see Table IV. TomTom data is computed based on all vehicles traveling that segment (with TomTom navigation enabled) averaged over $15\ mins$. A similar methodology is used for the SUMO vehicles to compute their average velocity. In the case of the SPM, a weighted average of traffic flow regions is used. In the free flow region vehicles travel with $v_A = 50\ km/h$, in the moving queue it is v_C, which is also $50\ km/h$ using trapezoidal MFD, and $v_J = 0\ km/h$ in the stationary queue. The $15\ mins$ averaged velocity on an SPM is

$$
\begin{aligned}
&\bar{v}_{SPM}\\
&= \frac{\Delta t}{15 \cdot 60}\\
&\cdot \sum_{\tau=0}^{\frac{15 \cdot 60}{\Delta t}} \frac{v_A(\tau)(l_l - l_q(\tau)) + v_C(\tau)(l_q(\tau) - l_{W_1}(\tau)) + v_J(\tau)l_{W_1}(\tau)}{l_l}.
\end{aligned}
$$

(17)

The FCD velocities tend to be higher both upstream and downstream compared to the simulated ones. The difference from the ground truth for SUMO is more significant than the SPM. Thus, it can be concluded that the accuracy of the
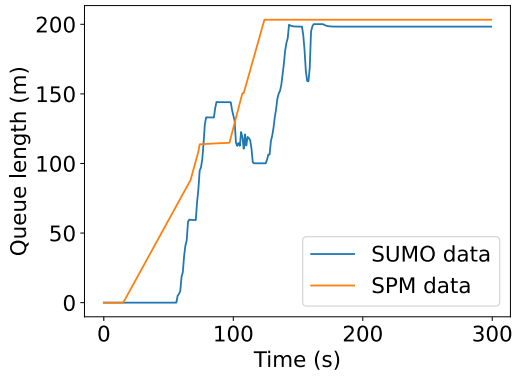
Fig. 13. Cumulated queue growth.

TABLE V
CONGESTION PATH. THE LINKS ARE ORDERED BY THE
TIME INSTANT THEY GET FULLY CONGESTED

SUMO		SPM	
Link ID	Congestion time (s)	Link ID	Congestion time (s)
IKa	76	IK	69
FI	134	FI	106
DF	143	DF	122

TABLE VI
ROOT MEAN SQUARE ERROR OF SUMO AND SPM QUEUE
LENGTH RESULTS IN THE EXPERIMENTAL NETWORK

Link ID	10% turning left	15% turning left	Jam propagation
DF	0.111	0.248	0.787
FG	0.424	0.435	0.208
FI	0.409	0.524	0.696
IK(a)	0.277	0.361	1.113
Average	0.293	0.451	0.423

mesoscopic simulation is comparable to the microscopic one (both with default settings).

In the following scenario, an accident is simulated 100 m downstream of the intersection (Link IKa) while the turning rate left is 10%. The queue lengths on the affected road links are summarized in Figure 12. Before Link IKa and FI get fully congested, the turning lane can empty twice. Then, as Link FI gets full, the queue starts accumulating on Link DF, too, blocking entry to Link FG. Thus, in the steady state, the left turning lane is empty, while there is a queue spanning over multiple links in the forward direction upstream of the accident. In both simulations, the order in which links get blocked is the same. However, it is faster in the SPM case, see Table V. The cumulated queue length (Figure 13) is more steady in the mesoscopic model, but in both cases, the queue growth stops (around 70 s) when the traffic light at Link BD stops incoming traffic. The root mean square errors (RMSE) are reported in Table VI.

IV. CONCLUSION

In the paper, the network-level extension of the shockwave profile model was presented. The main purpose of this extension is to create a general purpose mesoscopic traffic model that is computationally more efficient than microscopic simulation but still capable of accurately capturing the fluctuations of

traffic flow. The road topology is modeled as a directed graph. The model can be easily calibrated using some rule of thumb for the link fundamental diagram, turning rates from FCD data, and perimeter inflows from either scaled-up FCD data or traffic counts. Although the proposed model was presented in a jam-propagation detection context, it can be used for alternative purposes too. The SPM gives a good trade-off between simulation speed, calibration effort, and accuracy compared to microsimulation. In the jam-propagation context, the proposed model outperformed the cell transmission model, as the shockwave profile model better utilizes the information provided by the macroscopic fundamental diagram. Additionally, road links can be handled in a spatially continuous way, and there is no need for the discretization to cells.

Results of the numerical simulations suggest that the SPM model can accurately predict queue length growth and dissipation at signalized intersections. For unsignalized links, the queuing model can only predict average queues. On the other hand, for large networks, where the modeled queue is several links downstream, the inflow of the model gets less accurate: minor deviations and the stochasticity of the real traffic accumulate at this point. Therefore, it is better to discretize the network into smaller sub-networks. The model could accurately detect when some accident happened, modeling the rapid growth of queues and gridlock formation. The model can also capture recurrent events in the form of fluctuating queues in front of traffic lights and detect anomalies (i.e., gridlock) in case of an incorrect traffic light program or insufficient turning lane capacity. Compared to benchmarks, the SPM is 2-5 times more accurate in predicting queue lengths. Since jam propagation is derived from the queue length estimates, the proposed model can better predict both the speed and direction of traffic jam growth compared to the CTM.

The model can be used to find bottlenecks and incorrect signal programs by means of arbitrary traffic blockages and fictitious traffic flows. In the same vein, congestion dissipation can be modeled too. Additionally, the model can be used to forecast traffic states. Therefore, it can act as a basis for model-based predictive traffic control algorithms to remedy gridlock formation.

REFERENCES

[1] K. Saw, B. Katti, and G. Joshi, "Literature review of traffic assignment: Static and dynamic," *Int. J. Transp. Eng.*, vol. 2, no. 4, pp. 339–347, 2015.

[2] M. Maciejewski, "A comparison of microscopic traffic flow simulation systems for an urban area," *Transp. Problem*, vol. 5, pp. 27–38, Jan. 2010.

[3] C. Osorio and K. Nanduri, "Energy-efficient urban traffic management: A microscopic simulation-based approach," *Transp. Sci.*, vol. 49, no. 3, pp. 637–651, Aug. 2015.

[4] X. Ma, J. Jin, and W. Lei, "Multi-criteria analysis of optimal signal plans using microscopic traffic models," *Transp. Res. D, Transp. Environ.*, vol. 32, pp. 1–14, Oct. 2014.

[5] S. Dorokhin, A. Artemov, D. Likhachev, A. Novikov, and E. Starkov, "Traffic simulation: An analytical review," *IOP Conf., Mater. Sci. Eng.*, vol. 918, no. 1, Sep. 2020, Art. no. 012058.

[6] J. Maroto, E. Delso, J. Felez, and J. Ma. Cabanellas, "Real-time traffic simulation with a microscopic model," *IEEE Trans. Intell. Transp. Syst.*, vol. 7, no. 4, pp. 513–527, Dec. 2006.

[7] A. Pell, A. Meingast, and O. Schauer, "Trends in real-time traffic simulation," *Transp. Res. Proc.*, vol. 25, pp. 1477–1484, Jan. 2017.

[8] A. Saroj, S. Roy, A. Guin, M. Hunter, and R. Fujimoto, "Smart city real-time data-driven transportation simulation," in *Proc. Winter Simul. Conf. (WSC)*, Dec. 2018, pp. 857–868.

[9] B. Varga, M. Pereira, B. Kulcsár, L. Pariota, and T. Péni, "Data-driven distance metrics for kriging-short-term urban traffic state prediction," *IEEE Trans. Intell. Transp. Syst.*, vol. 24, no. 6, pp. 6268–6279, Jun. 2023.

[10] F. A. Schiegg, J. Krost, S. Jesenski, and J. Frye, "A novel simulation framework for the design and testing of advanced driver assistance systems," in *Proc. IEEE 90th Veh. Technol. Conf. (VTC-Fall)*, Sep. 2019, pp. 1–6.

[11] G. Khekare, P. Verma, U. Dhanre, S. Raut, and S. Sheikh, "The optimal path finding algorithm based on reinforcement learning," *Int. J. Softw. Sci. Comput. Intell.*, vol. 12, no. 4, pp. 1–18, Oct. 2020.

[12] F. Dembski, U. Wössner, and C. Yamu, "Digital twin, virtual reality and space syntax: Civic engagement and decision support for smart, sustainable cities," in *Proc. 12th Int. Space Syntax Conf.*, Beijing, China, 2019, pp. 8–13.

[13] X. Fang, T. Tettamanti, and A. C. Piazzi, "Online calibration of microscopic road traffic simulator," in *Proc. IEEE 18th World Symp. Appl. Mach. Intell. Informat. (SAMI)*, Jan. 2020, pp. 275–280.

[14] L. Bao, Q. Wang, and Y. Jiang, "Review of digital twin for intelligent transportation system," in *Proc. Int. Conf. Inf. Control, Electr. Eng. Rail Transit (ICEERT)*, Oct. 2021, pp. 309–315.

[15] M. Deveci, D. Pamucar, I. Gokasar, M. Koppen, and B. B. Gupta, "Personal mobility in metaverse with autonomous vehicles using q-rung orthopair fuzzy sets based OPA-RAFSI model," *IEEE Trans. Intell. Transp. Syst.*, early access, Jul. 12, 2022, doi: 10.1109/TITS.2022.3186294.

[16] T. Tettamanti, M. Szalai, S. Vass, and V. Tihanyi, "Vehicle-in-the-loop test environment for autonomous driving with microscopic traffic simulation," in *Proc. IEEE Int. Conf. Veh. Electron. Saf. (ICVES)*, Sep. 2018, pp. 1–6.

[17] M. Szalai, B. Varga, T. Tettamanti, and V. Tihanyi, "Mixed reality test environment for autonomous cars using unity 3D and SUMO," in *Proc. IEEE 18th World Symp. Appl. Mach. Intell. Informat. (SAMI)*, Jan. 2020, pp. 73–78.

[18] D. Nalic, A. Pandurevic, A. Eichberger, and B. Rogic, "Design and implementation of a co-simulation framework for testing of automated driving systems," *Sustainability*, vol. 12, no. 24, p. 10476, Dec. 2020.

[19] H. Li, D. Nalic, V. Makkapati, A. Eichberger, X. Fang, and T. Tettamanti, "A real-time co-simulation framework for virtual test and validation on a high dynamic vehicle test bed," in *Proc. IEEE Intell. Vehicles Symp. (IV)*, Jul. 2021, pp. 1132–1137.

[20] Y. Shi, Z. Liu, Z. Wang, J. Ye, W. Tong, and Z. Liu, "An integrated traffic and vehicle co-simulation testing framework for connected and autonomous vehicles," *IEEE Intell. Transp. Syst. Mag.*, vol. 14, no. 6, pp. 26–40, Nov. 2022.

[21] B. Varga, D. Doba, and T. Tettamanti, "Optimizing vehicle dynamics co-simulation performance by introducing mesoscopic traffic simulation," *Simul. Model. Pract. Theory*, vol. 125, May 2023, Art. no. 102739.

[22] X. Fang and T. Tettamanti, "Change in microscopic traffic simulation practice with respect to the emerging automated driving technology," *Periodica Polytechnica Civil Eng.*, vol. 66, no. 1, pp. 86–95, Sep. 2021.

[23] Z. Szalay, "Next generation X-in-the-Loop validation methodology for automated vehicle systems," *IEEE Access*, vol. 9, pp. 35616–35632, 2021.

[24] B. Németh, P. Gáspár, and Z. Bede, "Impact of automated vehicles using eco-cruise control on the traffic flow," *Periodica Polytechnica Transp. Eng.*, vol. 50, no. 1, pp. 1–10, Dec. 2021.

[25] S. P. Hoogendoorn and P. H. L. Bovy, "State-of-the-art of vehicular traffic flow modelling," *Proc. Inst. Mech. Eng., I, J. Syst. Control Eng.*, vol. 215, no. 4, pp. 283–303, Jun. 2001.

[26] L. A. Pipes, "An operational analysis of traffic dynamics," *J. Appl. Phys.*, vol. 24, no. 3, pp. 274–281, Mar. 1953.

[27] S. Krauß, "Towards a unified view of microscopic traffic flow theories," *IFAC Proc. Volumes*, vol. 30, no. 8, pp. 901–905, Jun. 1997.

[28] J. J. Olstam and A. Tapani, "Comparison car-following models," Swedish Nat. Road Transp. Res. Inst., Linköping, Sweden, Tech. Rep. 960A, 2004.

[29] K. Li and P. Ioannou, "Modeling of traffic flow of automated vehicles," *IEEE Trans. Intell. Transp. Syst.*, vol. 5, no. 2, pp. 99–113, Jun. 2004.

[30] R. E. Chandler, R. Herman, and E. W. Montroll, "Traffic dynamics: Studies in car following," *Operations Res.*, vol. 6, no. 2, pp. 165–184, Apr. 1958.

[31] C. F. Daganzo, "The cell transmission model—Part II: Network traffic," *Transp. Res. B, Methodol.*, vol. 29, no. 2, pp. 79–93, Apr. 1995.

[32] K. Nagel, "Particle hopping models and traffic flow theory," *Phys. Rev. E, Stat. Phys. Plasmas Fluids Relat. Interdiscip. Top.*, vol. 53, no. 5, pp. 4655–4672, May 1996.

[33] N. E. Lownes and R. B. Machemehl, "VISSIM: A multi-parameter sensitivity analysis," in *Proc. Winter Simul. Conf.*, Dec. 2006, pp. 1406–1413.

[34] B. Varga, T. Tettamanti, B. Kulcsár, and X. Qu, "Public transport trajectory planning with probabilistic guarantees," *Transp. Res. B, Methodol.*, vol. 139, pp. 81–101, Sep. 2020.

[35] D. Helbing, *Verkehrsdynamik: Neue Physikalische Modellierungskonzepte*. New York, NY, USA: Springer-Verlag, 2013.

[36] S. P. Hoogendoorn and P. H. L. Bovy, "Continuum modeling of multiclass traffic flow," *Transp. Res. B, Methodol.*, vol. 34, no. 2, pp. 123–146, Feb. 2000.

[37] M. J. Lighthill and G. B. Whitham, "On kinematic waves II. A theory of traffic flow on long crowded roads," *Proc. Roy. Soc. A, Math., Phys. Eng. Sci.*, vol. 229, no. 1178, pp. 317–345, 1955.

[38] H. J. Payne, "Model of freeway traffic and control," *Mathematical Model of Public System*. La Jolla, CA, USA: Simulation Councils, Inc, 1971, pp. 51–61.

[39] A. Kotsialos, M. Papageorgiou, and A. Messmer, "Optimal coordinated and integrated motorway network traffic control," in *Proc. 14th Int. Symp. Transp. Traffic TheoryTransp. Res. Inst.*, 1999, pp. 621–644.

[40] J. D. D. Ortázar and L. G. Willumsen, *Modelling Transport*, 4th ed. Hoboken, NJ, USA: Wiley, 2011.

[41] H. S. Mahmassani, M. Saberi, and A. Zockaie, "Urban network gridlock: Theory, characteristics, and dynamics," *Proc. Social Behav. Sci.*, vol. 80, pp. 79–98, Jul. 2013.

[42] M. Saberi et al., "A simple contagion process describes spreading of traffic jams in urban networks," *Nature Commun.*, vol. 11, no. 1, p. 1616, Apr. 2020.

[43] G. Zeng et al., "Switch between critical percolation modes in city traffic dynamics," *Proc. Nat. Acad. Sci. USA*, vol. 116, no. 1, pp. 23–28, Jan. 2019.

[44] D. Li et al., "Percolation transition in dynamical traffic network with evolving critical bottlenecks," *Proc. Nat. Acad. Sci. USA*, vol. 112, no. 3, pp. 669–672, Jan. 2015.

[45] B. Anbaroglu, B. Heydecker, and T. Cheng, "Spatio-temporal clustering for non-recurrent traffic congestion detection on urban road networks," *Transp. Res. C, Emerg. Technol.*, vol. 48, pp. 47–65, Nov. 2014.

[46] H. Nguyen, W. Liu, and F. Chen, "Discovering congestion propagation patterns in spatio-temporal traffic data," *IEEE Trans. Big Data*, vol. 3, no. 2, pp. 169–180, Jun. 2017.

[47] A. M. Nagy and V. Simon, "Improving traffic prediction using congestion propagation patterns in smart cities," *Adv. Eng. Informat.*, vol. 50, Oct. 2021, Art. no. 101343.

[48] C. Molinero, R. Murcio, and E. Arcaute, "The angular nature of road networks," *Sci. Rep.*, vol. 7, no. 1, p. 4312, Jun. 2017.

[49] C. Li, W. Yue, G. Mao, and Z. Xu, "Congestion propagation based bottleneck identification in urban road networks," *IEEE Trans. Veh. Technol.*, vol. 69, no. 5, pp. 4827–4841, May 2020.

[50] L. X. Pang, S. Chawla, W. Liu, and Y. Zheng, "On detection of emerging anomalous traffic patterns using GPS data," *Data Knowl. Eng.*, vol. 87, pp. 357–373, Sep. 2013.

[51] Z. Chen, Y. Yang, L. Huang, E. Wang, and D. Li, "Discovering urban traffic congestion propagation patterns with taxi trajectory data," *IEEE Access*, vol. 6, pp. 69481–69491, 2018.

[52] S. Kaffash, A. T. Nguyen, and J. Zhu, "Big data algorithms and applications in intelligent transportation system: A review and bibliometric analysis," *Int. J. Prod. Econ.*, vol. 231, Jan. 2021, Art. no. 107868.

[53] J. Long, Z. Gao, H. Ren, and A. Lian, "Urban traffic congestion propagation and bottleneck identification," *Sci. China F, Inf. Sci.*, vol. 51, no. 7, pp. 948–964, Jul. 2008.

[54] X. Wu and H. X. Liu, "A shockwave profile model for traffic flow on congested urban arterials," *Transp. Res. B, Methodol.*, vol. 45, no. 10, pp. 1768–1786, Dec. 2011.

[55] P. Hunt, D. Robertson, R. Bretherton, and R. Winton, "Scoot—A traffic responsive method of coordinating signals," Transp. Road Res. Lab., Crowthorne, U.K., Tech. Rep. LR 1014 Monograph, 1981.

[56] K. Aboudolas, M. Papageorgiou, and E. Kosmatopoulos, "Store-and-forward based methods for the signal control problem in large-scale congested urban road networks," *Transp. Res. C, Emerg. Technol.*, vol. 17, no. 2, pp. 163–174, Apr. 2009.

[57] S. Lin, B. De Schutter, Y. Xi, and H. Hellendoorn, "Model predictive control for urban traffic networks via MILP," in *Proc. Amer. Control Conf.*, Jul. 2010, pp. 2272–2277.

[58] E. C. Matsoukis and P. Michalopoulos, "Road traffic assignment—A review: Part II: Equilibrium methods," *Transp. Planning Technol.*, vol. 11, no. 2, pp. 117–135, 1986.

[59] M. A. Boon and M. Mandjes, "Generalized gap acceptance models for unsignalized intersections," *Math. Methods Oper. Res.*, vol. 89, no. 3, pp. 385–409, Jun. 2019.

[60] W. Siegloch, "Ein richtlinienvorschlag zur leistungsermittlung an knotenpunkten ohne lichtsignalsteuerung (capacity calculations for unsignalized intersections)," *Strassenverkehrstechnik*, vol. 1, no. 154, p. 173S, 1974.

[61] M. Krbálek, T. Hobza, M. Patočka, M. Krbálková, J. Apeltauer, and N. Groverová, "Statistical aspects of gap-acceptance theory for unsignalized intersection capacity," *Phys. A, Stat. Mech. Appl.*, vol. 594, May 2022, Art. no. 127043.

[62] A. Weinert, "Estimation of critical gaps and follow-up times at rural unsignalized intersections in Germany," in *Proc. 4th Int. Symp. Highway Capacity*, 2000, pp. 409–421.

[63] P. A. Lopez et al., "Microscopic traffic simulation using SUMO," in *Proc. 21st Int. Conf. Intell. Transp. Syst. (ITSC)*, Nov. 2018, pp. 2575–2582.

[64] W. Brilon, N. Wu, and L. Bondzio, "Unsignalized intersections in Germany—A state of the art 1997," in *Proc. 3rd Int. Symp. Intersections Traffic Signals*, 1997, pp. 61–70.

[65] R. Akcelik, "The highway capacity manual delay formula for signalized intersections," *ITE J.*, vol. 58, no. 3, pp. 23–27, 1988.

[66] H. C. Manual, *Highway Capacity Manual*, vol. 2. Washington, DC, USA: Transportation Research Board, 2000.

[67] R. Yin, N. Zheng, and Z. Liu, "Estimating fundamental diagram for multi-modal signalized urban links with limited probe data," *Phys. A, Stat. Mech. Appl.*, vol. 606, Nov. 2022, Art. no. 128091. [Online]. Available: https://www.sciencedirect.com/science/article/pii/S0378437122006768

[68] I. Yperman, S. Logghe, and B. Immers, "The link transmission model: An efficient implementation of the kinematic wave theory in traffic networks," in *Proc. 10th EWGT Meeting*, vol. 24. Poznań, Poland, 2005, pp. 123–127.

[69] N. G. Eissfeldt, "Vehicle-based modelling of traffic. Theory and application to environmental impact modelling," Ph.D. dissertation, Fac. Math. Natural Sci., Dept. Math. Comput. Sci., Inst. Comput. Sci., Universität zu Köln, Cologne, Germany, 2004.

Balázs Varga received the M.Sc. degree in vehicle engineering and the Ph.D. degree in traffic engineering from the Budapest University of Technology and Economics, Budapest, Hungary, in 2015 and 2021, respectively. He was a Post-Doctoral Researcher with the Chalmers University of Technology, Gothenburg, Sweden, in 2021. He is currently a Researcher with the Budapest University of Technology and Economics. He has over 30 scientific publications. His main research interests include the modeling and control of urban traffic networks.

Tamás Tettamanti received the M.Sc. and Ph.D. degrees in traffic engineering from the Budapest University of Technology and Economics, Hungary, in 2007 and 2013, respectively. He is currently an Associate Professor with the Faculty of Transportation Engineering and Vehicle Engineering, Budapest University of Technology and Economics. He participates in research and industrial projects both as a researcher and a project coordinator. He is the coauthor of over 160 scientific papers, two patents, and several books. His main research interests include road traffic modeling, estimation and control in the cooperative, connected and automated mobility (CCAM) field, and related co-simulation technology developments. He is a member of the Public Body of the Hungarian Academy of Sciences.